

1 Effects of aquifer geometry on seawater intrusion in annulus  
2 segment island aquifers  
3

4 Zhaoyang Luo<sup>1,2</sup>, Jun Kong<sup>1,3,#</sup>, Chengji Shen<sup>1</sup>, Pei Xin<sup>1</sup>, Chunhui Lu<sup>1</sup>, Ling Li<sup>4</sup>,  
5 David Andrew Barry<sup>2</sup>  
6

7 <sup>1</sup>State Key Laboratory of Hydrology-Water Resources and Hydraulic Engineering, Hohai  
8 University, Nanjing, China  
9

10 <sup>2</sup>Ecological Engineering Laboratory (ECOL), Environmental Engineering Institute (IIE),  
11 Faculty of Architecture, Civil and Environmental Engineering (ENAC), École Polytechnique  
12 Fédérale de Lausanne (EPFL), Lausanne, Switzerland  
13

14 <sup>3</sup>Jiangsu Key Laboratory of Coast Ocean Resources Development and Environment Security,  
15 Hohai University, Nanjing, China  
16

17 <sup>4</sup>School of Engineering, Westlake University, Hangzhou, China  
18

19 <sup>#</sup>Corresponding author: Jun Kong ([kongjun999@126.com](mailto:kongjun999@126.com))  
20

21 Resubmitted to *Hydrology and Earth System Sciences* on 26 November 2021

Deleted: 8

Deleted: 30

Formatted: Not Highlight

24 **Abstract**

25 Seawater intrusion in island aquifers was considered analytically, specifically for annulus  
26 segment aquifers (ASAs), i.e., aquifers that (in plan) have the shape of an annulus segment.

27 Based on the Ghijben-Herzberg and hillslope-storage Boussinesq equations, analytical  
28 solutions were derived for steady-state seawater intrusion in ASAs, with a focus on the  
29 freshwater-seawater interface and its corresponding watertable elevation. Predictions of the  
30 analytical solutions compared well with experimental data, and so they were employed to  
31 investigate the effects of aquifer geometry on seawater intrusion in island aquifers. Three

32 different ASA geometries were compared: convergent (smaller side facing the lagoon, larger  
33 side is the internal no-flow boundary, flow converges towards the lagoon), rectangular and  
34 divergent (smaller side is the internal no-flow boundary, larger side facing the sea, flow  
35 diverges towards the sea). Depending on the aquifer geometry, seawater intrusion was found

36 to vary greatly, such that the assumption of a rectangular aquifer to model an ASA can lead to  
37 poor estimates of seawater intrusion. Other factors being equal, compared with rectangular  
38 aquifers, seawater intrusion is more extensive and watertable elevation is lower in divergent  
39 aquifers, with the opposite tendency in convergent aquifers. Sensitivity analysis further  
40 indicated that the effects of aquifer geometry on seawater intrusion and watertable elevation  
41 vary with aquifer width and distance from the circle center to the inner arc (the lagoon

42 boundary for convergent aquifers or the internal no-flow boundary for divergent aquifers). A  
43 larger aquifer width and distance from the circle center to the inner arc weaken the effects of  
44 aquifer geometry and hence differences in predictions for the three geometries become less

Formatted: Not Highlight

Formatted: Not Highlight

Deleted: while

46 pronounced

Deleted: Page Break

47 **Keywords:** sharp-interface; steady-state analytical solution; atoll aquifer; annulus segment

Formatted: Space Before: 24 pt

48 aquifer, seawater intrusion

49 **Key Points**

- 50 ➤ Analytical solutions of steady-state seawater intrusion were derived for annulus segment
- 51 aquifers
- 52 ➤ Among three different aquifer geometries, divergent aquifers have the lowest watertable
- 53 and hence the most extensive seawater intrusion
- 54 ➤ Aquifer geometry effects on seawater intrusion depend on the aquifer width and distance
- 55 from the circle center to the inner arc

## 1. Introduction

Islands are extensively distributed throughout the world's oceans. Unfortunately, their groundwater resources are impacted by sea-level rise and increased demands. According to a recent estimate, there are approximately 65 million people living in oceanic islands where groundwater may be the only source of freshwater (Thomas et al., 2020). Fresh groundwater stored on oceanic islands is mainly from precipitation (usually in the form of a freshwater lens) and its availability varies due to different factors, e.g., island topography, rainfall patterns, tides, episodic storms and human activities (White & Falkland, 2010; Storlazzi et al., 2018). Seawater intrusion is thus an important issue due to its deleterious effect on oceanic island freshwater storage (e.g., Werner et al., 2017; Lu et al., 2019; Memari et al., 2020).

Over the past few decades, seawater intrusion in oceanic islands has been extensively investigated in field observations (e.g., Röper et al., 2013; Post et al., 2019), laboratory experiments (e.g., Stoeckl et al., 2015; Bedekar et al., 2019; Memari et al., 2020), numerical simulations (e.g., Lam, 1974; Gingerich et al., 2017; Liu & Tokunaga, 2019) and analytical solutions (e.g., Fetter, 1972; Ketabchi et al., 2014; Lu et al., 2019). Among these, analytical solutions are effective tools to assess the extent of seawater intrusion (i.e., the location of the freshwater-seawater interface), although they cannot incorporate complex factors (e.g., dispersive mixing and transient oceanic dynamics) (Werner et al., 2013). The advantages of analytical solutions are that they are computationally efficient, can be used as test cases for numerical models, and can reveal the explicit relationships between parameters that influence seawater intrusion (e.g., Fetter, 1972; Ketabchi et al., 2014; Liu et al., 2014; Lu et al., 2019).

**Deleted:** In contrast to coastal aquifers where seawater intrudes into freshwater from one direction only, seawater intrusion occurs from four directions for narrow strip islands and from all directions for circular islands.

**Deleted:** ;

83 Based on the Dupuit-Forchheimer approximation (i.e., ignoring vertical flow) and the  
84 Ghijben-Herzberg equation (Drabbe & Badon Ghijben, 1889, English translation given by  
85 Post (2018); Herzberg, 1901), Fetter (1972) presented analytical solutions describing the  
86 freshwater-seawater interface location and watertable elevation in a circular island. Bailey et  
87 al. (2010) further compared these single-layered analytical solutions with field measurements,  
88 indicating that the analytical solutions perform well in estimating the freshwater-seawater  
89 interface location and watertable elevation. Fetter's solutions formed the foundation for many  
90 subsequent analytical studies on seawater intrusion in island aquifers. Again, for a single  
91 layer, Chesnaux and Allen (2008) and Greskowiak et al. (2013) developed analytical solutions  
92 to predict the steady-state groundwater age distribution in freshwater lenses. In addition, using  
93 single-layered analytical solutions, Morgan and Werner (2014) proposed vulnerability  
94 indicators of freshwater lenses under sea-level rise and recharge change.

95 Since aquifers are usually heterogeneous, the single-layer analytical solutions were  
96 subsequently extended to two-layered island aquifers. Vacher (1988) derived solutions for the  
97 freshwater-seawater interface location and watertable elevation for infinite-strip islands  
98 composed of different layers. Dose et al. (2014) conducted laboratory experiments to validate  
99 and confirm the reliability of analytical solutions proposed by Fetter (1972) and Vacher  
100 (1988). Ketabchi et al. (2014) extended Fetter's analytical solutions to calculate the  
101 freshwater-seawater interface location and watertable elevation in two-layered circular islands  
102 subject to sea-level rise. Their results indicated that land-surface inundation caused by sea-  
103 level rise has a considerable impact on fresh groundwater lenses. Recently, Lu et al. (2019)

104 derived analytical solutions for the freshwater-seawater interface location and watertable  
105 elevation for both strip and circular islands with two adjacent layers, i.e., a less permeable  
106 slice along the shoreline of an island, and a more permeable zone inland.

107 All the abovementioned analytical solutions apply to either strip or circular islands.  
108 According to the classification of sand dunes developed by Stuyfzand (1993; 2017), there are  
109 different island layouts that should be considered, e.g., where the shape of the island is an  
110 annulus segment, instead of a strip or circular disk (Figure 1). Annulus segment-shaped  
111 islands are found in various atolls (i.e., circular chains of islands surrounding a central  
112 lagoon) as found in the Pacific and Indian Oceans (Werner et al., 2017; Duvat, 2019).  
113 Nevertheless, analytical solutions of seawater intrusion are not yet available for annulus  
114 segment aquifers (ASAs). In general, ASAs are conceptually treated as a 2D cross section,  
115 similar to strip islands (e.g., Ayers & Vacher, 1986; Underwood et al., 1992; Bailey et al.,  
116 2009; Werner et al., 2017). Evidently, topography plays an important role in groundwater flow  
117 and hence seawater intrusion (e.g., Zhang et al., 2016; Liu & Tokunaga, 2019). It remains  
118 unclear whether analytical solutions of seawater intrusion for strip islands are appropriate for  
119 ASAs. It is ~~also~~ unclear how island geometry affects the freshwater-seawater interface  
120 location and watertable elevation of ASAs.

121 In this study, analytical solutions are derived for steady-state seawater intrusion for ASAs,  
122 with a focus on the freshwater-seawater interface location and its corresponding watertable  
123 elevation. After comparing their predictions with experimental data (Memari et al., 2020), the  
124 analytical solutions are employed to investigate the effects of aquifer geometry on the

Deleted: moreover

Deleted: additionally

127 freshwater-seawater interface location and watertable elevation in ASAs.

## 128 2. Conceptual Model

129 Figure 2 shows the conceptual model of an ASA (a slice of an atoll island). The plan  
130 view of the model domain is represented as a sector ( $EFGH$ ) with an angle  $\theta$  (Figure 2a).

131 The sea ( $EF$ ) and lagoon ( $HG$ ) boundaries are located at  $L + L_0$  [L] and  $L_0$  [L] from the circle  
132 center, respectively. Since the longitudinal length is usually much longer than the lateral  
133 length for an atoll island (Werner et al., 2017), seawater intrusion from the lateral sides ( $EH$   
134 and  $FG$ , Figure 2a) is negligible in comparison to the longitudinal side, especially for the  
135 middle portion of an ASA. Therefore,  $EH$  and  $FG$  are treated as lateral no-flow boundaries.

136 Note that treating the lateral sides as no-flow boundaries is often used in studies of freshwater  
137 lenses on atoll islands (e.g., Ayers & Vacher, 1986; Underwood et al., 1992; Bailey et al.,  
138 2009; Werner et al., 2017). The lateral vertical cross section of the model domain is  
139 conceptualized as a rectangle ( $ABCD$ ) along the radial direction with dimensions of  $L$  [L]  
140 (width)  $\times$   $d$  [L] (height) (Figure 2b, c).  $AD$  is the impermeable base while  $BC$  is the land  
141 surface through which aquifer recharge flows.

142 Both the sea and lagoon water levels are set to  $H_s$  [L], which results in an internal no-  
143 flow boundary (water divide, where the slope of the watertable is zero) between the sea and  
144 lagoon (location of the  $z$ -axis in Figure 2b,c). The segment between the sea and the internal  
145 no-flow boundary is referred to as Unit 1, whereas the segment between the internal no-flow  
146 and lagoon boundaries is referred to as Unit 2 (Figure 2). The widths of Units 1 and 2 are  $l_1$   
147 [L] and  $l_2$  [L], respectively. In addition, the flow is asymmetrical in Units 1 and 2, with

Moved down [1]: Radial flow only is considered.

Formatted: Font color: Text 1

Deleted: side view

150 divergent flow (the aquifer length  $w$  [L] increases along the flow direction) in Unit 1 and  
151 convergent flow ( $w$  decreases along the flow direction) in Unit 2.

152 The  $r$ - $z$  coordinate origin is placed at the intersection of the internal no-flow boundary  
153 and impermeable base, with the  $r$ -axis pointing to the circle center (radial direction) and the  $z$ -  
154 axis pointing vertically upward. Further,  $\phi$  [L] is the watertable height,  $h$  [L] is the  
155 vertical distance between the watertable and the interface,  $h_s$  [L] is the vertical distance  
156 between the sea level and the interface, and  $h_c = H_s - h_s$  [L] is the vertical distance from the  
157 impermeable base to the interface for given  $r$  (Figure 2b,c). Constant recharge into the  
158 saturated zone,  $N$  [LT<sup>-1</sup>], is assumed. There are two possibilities for the interface tip (i.e., the  
159 location where the freshwater-seawater interface connects to the  $z$ -axis or the bottom  
160 boundary): above the aquifer bed (Figure 2b) or on the aquifer bed (Figure 2c). The  $r$ -  
161 coordinates of the interface tip in Units 1 and 2 are denoted as  $r_{t1}$  [L] and  $r_{t2}$  [L], respectively  
162 (Figure 2c). Note that  $r_{t1} = r_{t2} = 0$  when the interface tip is above the aquifer bed, as in Figure  
163 2b.

164 Consistent with previous studies (e.g., Ketabchi et al., 2014; Lu et al., 2016; 2019), the  
165 following assumptions are made: (1) steady-state flow, (2) sharp freshwater-seawater  
166 interface, (3) homogeneous and isotropic aquifer with a horizontal bottom, (4) rainfall is equal  
167 to the replenishment of the saturated zone with a magnitude that is less than the saturated  
168 hydraulic conductivity (else overland flow will appear), (5) vertical flow in the saturated zone  
169 is negligible (the Dupuit-Forchheimer approximation), and (6) the same velocity is assumed  
170 on the arc ( $w$ ) for a given radial distance  $r$ , leading to radial flow only. Based on this last

Deleted:  $x$

Deleted:  $x$

Deleted:  $x$

Deleted:  $x$

Deleted:  $x_{t1}$

Deleted:  $x_{t2}$

Deleted:  $x_{t1}$

Deleted:  $x_{t2}$

Deleted: flat

Deleted: negligible unsaturated flow

Deleted: , (5) recharge rainfall

Deleted: and

Deleted: while

Deleted: following ponding

Deleted: and

Deleted: 6

Deleted: 7

Deleted: Radial flow only is considered.

Moved (insertion) [1]



189 assumption, the 3D flow problem can be simplified to 1D, making it possible to consider  
 190 geometry effects analytically (Fan & Bras, 1998; Paniconi et al., 2003; Troch et al., 2003).

### 191 3. Analytical Solutions

192 Under the abovementioned assumptions, groundwater flow in an ASA (Figure 2) can be  
 193 described as (Fan & Bras, 1998; Paniconi et al., 2003; Troch et al., 2003),

$$194 \quad -\frac{d}{dr}(wq) + Nw = 0 \quad (1)$$

195 where  $q$  [ $L^2T^{-1}$ ] is the radial flux per unit length along the radial direction  $r$  [L]. Equation  
 196 (1) is a special case of the hillslope-storage Boussinesq equation proposed by Troch et al.

197 (2003). Paniconi et al. (2003) validated the hillslope-storage Boussinesq equation by  
 198 comparing it with a 3D Richards' equation model and found that predictions of the hillslope-  
 199 storage Boussinesq equation matched well those of the 3D model for seven different  
 200 geometries. For conciseness, readers are referred to Paniconi et al. (2003) for more details

201 about the validation. Subsequently, the hillslope-storage Boussinesq equation was used to for  
 202 different analyses (Hilberts et al., 2005, 2007; Hazenberg et al., 2015, 2016; Kong et al.,  
 203 2016; Luo et al., 2018), all of which focus on hillslope aquifers where the aquifer bottom is  
 204 usually sloping. The hillslope-storage Boussinesq equation assumes that groundwater flow is  
 205 parallel to the aquifer bottom (the Dupuit-Forchheimer approximation). Therefore, it can be  
 206 applied to coastal unconfined aquifers where the aquifer bottom slope is usually mild (Lu et  
 207 al., 2016).

208 According to Darcy's law and the Dupuit-Forchheimer approximation, the freshwater  
 209 flux in the aquifer segment between the seaward boundary and interface tip can be calculated

- Deleted: (
- Deleted: 7
- Deleted: 6)
- Deleted:
- Deleted: Groundwater
- Field Code Changed
- Deleted:  $-\frac{\partial}{\partial x}(wq) + Nw = \frac{\partial S}{\partial t}$
- Formatted: Normal
- Deleted: Darcy
- Deleted: the aquifer
- Deleted: ,
- Deleted: x
- Deleted: represents the distance from the circle center to the arc,  $S$  [ $L^2$ ] is the total water storage per unit distance along the aquifer, and  $t$  [T] is time.
- Deleted: the so-called
- Deleted: the
- Deleted: that and was first
- Deleted: For a given radial distance  $x$ , this equation assumes that the velocity is the same everywhere on the arc ( $w$ ). Based on...
- Deleted: equation (1)
- Deleted: equation (1)
- Deleted: nine
- Deleted:
- Deleted: equation (1)
- Deleted: further
- Deleted: . A
- Deleted: the existing applications based on the hillslope-...
- Deleted: be easily extended
- Deleted: pretty
- Deleted: in the saturated zone unconfined slop pretty mild
- Deleted: mild, even horizontal
- Deleted: At steady state, equation (1) reduces to, ...

250 as ( $\phi$  is independent of  $z$ ),

$$251 \quad q = -\int_{h_c}^{\phi} K_s \frac{d\phi}{dr} dz = -K_s (\phi - h_c) \frac{d\phi}{dr} \quad (2)$$

252 where  $K_s$  [ $LT^{-1}$ ] is the saturated hydraulic conductivity.

### 253 3.1. Interface Tip above the Aquifer Bed

254 We first consider the situation where the interface tip is above the aquifer bed (Figure

255 2b). In Unit 1 where  $w = \theta(L_0 + l_2 - r)$ , substituting equation (2) into equation (1) and then

256 integrating gives,

$$257 \quad -\frac{1}{2}[(L_0 + l_2 - r)^2 - (L_0 + l_2)^2]N = -(L_0 + l_2 - r)K_s (\phi - h_c) \frac{d\phi}{dr} \quad (3)$$

258 According to the Ghijben-Herzberg equation, the vertical thickness of the freshwater zone ( $h$ )

259 in the interface zone is given by,

$$260 \quad h = \phi - h_c = (1 + \alpha)(\phi - H_s) \quad (4)$$

261 where  $\alpha = \rho_f / (\rho_s - \rho_f)$  is the dimensionless density difference, and  $\rho_f$  [ $ML^{-3}$ ] and  $\rho_s$

262 [ $ML^{-3}$ ] are the freshwater and seawater densities, respectively. Substitution of equation (4)

263 into equation (3) yields,

$$264 \quad -\frac{1}{2}[(L_0 + l_2 - r)^2 - (L_0 + l_2)^2]N = -K_s (L_0 + l_2 - r)(1 + \alpha)(\phi - H_s) \frac{d\phi}{dr} \quad (5)$$

265 Rearranging equation (5) produces,

$$266 \quad -\frac{(L_0 + l_2 - r)N}{2} + \frac{N(L_0 + l_2)^2}{2(L_0 + l_2 - r)} = -K_s (1 + \alpha)(\phi - H_s) \frac{d\phi}{dr} \quad (6)$$

267 Integrating equation (6) leads to,

$$268 \quad -\frac{(L_0 + l_2)^2 N}{2} \ln(L_0 + l_2 - r) - \frac{1}{2}(L_0 + l_2)Nr + \frac{1}{4}Nr^2 + C_1 = -K_s (1 + \alpha) \frac{(\phi - H_s)^2}{2} \quad (7)$$

269 where  $C_1$  is the integration constant that is determined by the sea boundary condition (i.e.,

Deleted: 3

Deleted: 3

Deleted: 2

Deleted: 4

Deleted: 5

Deleted: 5

Deleted: 4

Deleted: 6

Deleted: 6

Deleted: 7

Deleted: 7

Deleted: 8

282  $r = -l_1, \phi = H_s$ ),

$$283 \quad C_1 = \frac{(L_0 + l_2)^2 N}{2} \ln(L_0 + l_2 + l_1) - \frac{1}{2}(L_0 + l_2)l_1 N - \frac{1}{4}l_1^2 N \quad (8)$$

284 The relation between  $h_s$  and  $\phi$  is given by,

$$285 \quad h_s = \alpha(\phi - H_s) \quad (9)$$

286 Combining equation (7) with equation (9) and eliminating  $\phi$  yields,

$$287 \quad -\frac{(L_0 + l_2)^2 N}{2} \ln(L_0 + l_2 - r) - \frac{1}{2}(L_0 + l_2)Nr + \frac{1}{4}Nr^2 + C_1 = -K_s(1 + \alpha)\frac{h_s^2}{2\alpha^2} \quad (10)$$

288 Equation (10) gives the freshwater-seawater interface location in Unit 1 once  $l_1$  and  $l_2$  are  
289 determined.

290 Equation (7) applies to Unit 2 by replacing  $C_1$  with  $C_2$ ,

$$291 \quad -\frac{(L_0 + l_2)^2 N}{2} \ln(L_0 + l_2 - r) - \frac{1}{2}(L_0 + l_2)Nr + \frac{1}{4}Nr^2 + C_2 = -K_s(1 + \alpha)\frac{(\phi - H_s)^2}{2} \quad (11)$$

292 where  $C_2$  is chosen to satisfy the lagoon boundary condition ( $r = l_2, \phi = H_s$ ),

$$293 \quad C_2 = \frac{(L_0 + l_2)^2 N}{2} \ln(L_0) + \frac{1}{2}(L_0 + l_2)l_2 N - \frac{1}{4}l_2^2 N \quad (12)$$

294 Combining equations (9) and (11) and eliminating  $\phi$  leads to,

$$295 \quad -\frac{(L_0 + l_2)^2 N}{2} \ln(L_0 + l_2 - r) - \frac{1}{2}(L_0 + l_2)Nr + \frac{1}{4}Nr^2 + C_2 = -K_s(1 + \alpha)\frac{h_s^2}{2\alpha^2} \quad (13)$$

296 Equation (13) gives the freshwater-seawater interface location in Unit 2 once  $l_2$  is

297 determined. Since the sea level and lagoon water level are the same, an internal no-flow

298 boundary exists between the sea and lagoon, i.e.,

$$299 \quad r = 0, (h_s)_{unit1} = (h_s)_{unit2} \quad (14)$$

300 where  $(h_s)_{unit1}$  and  $(h_s)_{unit2}$  represent  $h_s$  in Units 1 and 2, respectively.

315 Combining equations (10), (13) and (14) leads to expressions for  $l_1$  and  $l_2$ ,

$$316 \quad l_1 = L + L_0 - \sqrt{\frac{2LL_0 + L^2}{2\ln(L + L_0) - 2\ln(L_0)}} \quad (15)$$

$$317 \quad l_2 = \sqrt{\frac{2LL_0 + L^2}{2\ln(L + L_0) - 2\ln(L_0)}} - L_0 \quad (16)$$

318 As indicated by equations (15) and (16), the internal no-flow boundary between the sea and

319 lagoon only depends on  $L$  and  $L_0$ . For known  $l_1$  and  $l_2$ , equations (10) and (13) can be

320 employed to predict the freshwater-seawater interface location in Units 1 and 2, respectively.

321 Once the interface location is determined,  $h$  and  $\phi$  are given by,

$$322 \quad h = \frac{1 + \alpha}{\alpha} h_s \quad (17)$$

$$323 \quad \phi = \frac{h_s}{\alpha} + H_s \quad (18)$$

### 324 3.2. Interface Tip on the Aquifer Bed

325 When the interface tip is on the aquifer bed, the location of the internal no-flow

326 boundary remains the same as for the interface tip above the aquifer bed. The freshwater-

327 seawater interface for Units 1 and 2 can be determined by equations (10) and (13),

328 respectively. Then, from equation (17),  $h$  at the aquifer segment between the sea boundary and

329 the interface tip is determined. To calculate  $h$  for the aquifer segment between the interface tip

330 and the internal no-flow boundary, the  $r$ -coordinate of the interface tip is found. At the

331 interface tip of Unit 1 ( $r = r_{i1}$ ),

$$332 \quad h_s = H_s \quad (19)$$

$$333 \quad \phi = \frac{1 + \alpha}{\alpha} H_s \quad (20)$$

334 With equations (10) and (20),  $r_{i1}$  is given by,

Deleted: 11

Deleted: 14

Deleted: 15

Deleted: 16

Deleted: 17

Deleted: 16

Deleted: 17

Deleted: 11

Deleted: 14

Deleted: 18

Deleted: 19

Deleted: 11

Deleted: 4

Deleted: 18

Deleted: x

Formatted: Font: Italic

Formatted: Font: Italic

Formatted: Font: Italic, Subscript

Formatted: Subscript

Deleted:  $r = r_{i1}$

Deleted: 20

Deleted: 21

Deleted: 11

Deleted: 21

Deleted:  $x_{r1}$

$$-\frac{(L_0 + l_2)^2 N}{2} \ln(L_0 + l_2 - r_{i1}) - \frac{1}{2}(L_0 + l_2)Nr_{i1} + \frac{1}{4}Nr_{i1}^2 = -C_1 - K_s(1 + \alpha) \frac{H_s^2}{2\alpha^2} \quad (21)$$

Deleted: 22

Let,

$$a = \frac{1}{4}N \quad (22a)$$

Deleted: 23a

$$b = -\frac{1}{2}(L_0 + l_2)N \quad (22b)$$

Deleted: 23b

$$c = -\frac{(L_0 + l_2)^2 N}{2} \quad (22c)$$

Deleted: 23c

and

$$m = -C_1 - K_s(1 + \alpha) \frac{H_s^2}{2\alpha^2} \quad (22d)$$

Deleted: 23d

then equation (21) becomes,

Deleted: 22

$$ar_{i1}^2 + br_{i1} + c \ln(L_0 + l_2 - r_{i1}) = m \quad (23)$$

Deleted: 24

which is solved by a root-finding method.

The freshwater discharge for the aquifer segment between the interface tip and the internal no-flow boundary is calculated as,

$$-\frac{1}{2}[(L_0 + l_2 - r)^2 - (L_0 + l_2)^2]N = -(L_0 + l_2 - r)K_s\phi \frac{d\phi}{dr} \quad (24)$$

Deleted: 25

Repeating the steps from equations (3) to (7) gives,

Deleted: 4

$$-\frac{(L_0 + l_2)^2 N}{2} \ln(L_0 + l_2 - r) - \frac{1}{2}(L_0 + l_2)Nr + \frac{1}{4}Nr^2 + C_3 = -\frac{K_s}{2}\phi^2 \quad (25)$$

Deleted: 8

Deleted: 26

where  $C_3$  is determined by substituting equation (20) into equation (25). Then, equation (25)

Deleted: 21

can be adopted to calculate  $h$  for the segment between the interface tip and the internal no-

Deleted: 26

flow boundary where  $h = \phi$ .

Deleted: 26

Similarly, the  $x$ -coordinate of the interface tip in Unit 2 ( $x_{i2}$ ) is obtained by substituting

Deleted:  $x$

Deleted:  $x_{i2}$

391 equation (19) into equation (13). Then, the watertable ( $h$ ) of the aquifer segment between the  
392 interface tip and the internal no-flow boundary for Unit 2 is computed by repeating the steps  
393 from equations (21) to (25).

## 394 4. Results and Discussion

### 395 4.1. Validation of the Analytical Solutions

396 The analytical solutions were validated by comparing their predictions with experimental  
397 data compiled from Memari et al. (2020), who reported experiments carried out using a 15°  
398 radial tank. The tank contained three distinct chambers: internal no-flow boundary condition,  
399 porous medium and constant-head boundary condition (i.e., sea or lagoon). The internal no-  
400 flow and seaward boundaries were respectively located at 10 and 55.5 cm from the circle  
401 center, i.e., 45.5 cm from the internal no-flow boundary to the constant-head boundary along  
402 the radial direction. Note that the experimental tank corresponds to Unit 1 of the radial aquifer  
403 with  $l_1 = 45.5$  cm and  $l_2 = 0$ , so the analytical results were calculated using equations (10)  
404 and (23). The thicknesses of the porous medium and sea level were 28 and 25 cm,  
405 respectively, with  $K_s = 1.23 \times 10^{-2}$  m s<sup>-1</sup>. The measured saltwater and freshwater densities  
406 were respectively 1.015 and 0.999 g ml<sup>-1</sup>, leading to  $\alpha = 62$ . Two different recharge events  
407 with constant  $N$ ,  $2.46 \times 10^{-4}$  and  $1.08 \times 10^{-4}$  m s<sup>-1</sup>, were considered in the experiments.

408 Figure 3 shows the comparison between analytical and experimental results of the  
409 freshwater-seawater interface for different recharge events. In general, the analytical solution  
410 predicts the freshwater-seawater interface well for both recharge events, despite there being  
411 some differences between the analytical results and the measurements, particularly in the zone

Deleted: 20

Deleted: 14

Deleted: 22

Deleted: 26

Deleted: cm

Deleted: only

Deleted: 11

Deleted: 24

420 near the constant-head boundary ( $r = -45$  cm). These deviations are likely due to assumptions  
421 made in the analytical solution, i.e., (i) a sharp freshwater-seawater interface, (ii) ignoring the  
422 effect of freshwater discharge, and (iii) neglecting the vertical flow (the Dupuit-Forchheimer  
423 approximation).

Deleted: x

#### 424 4.2. Effects of Aquifer Geometry on Seawater Intrusion

425 Previous studies showed that boundary conditions play a critical role in estimates of  
426 seawater intrusion (Werner & Simmons, 2009; Lu et al., 2016). Therefore, the internal no-  
427 flow boundary between the sea and lagoon was examined for various ASAs. As indicated by

428 equations (15) and (16), this internal no-flow boundary depends only on  $L$  and  $L_0$ . The values

Deleted: 16

429 of  $l_1$  and  $l_2$  calculated respectively from equations (15) and (16) are shown in Figure 4 for

Deleted: 17

430 three typical values of  $L$  (500, 1000 and 2000 m) with  $L_0$  varying from  $10^2$  to  $10^6$  m. In

Deleted: 16

431 general, the internal no-flow boundary deviates from the middle of the ASA. When  $L_0$  is less

Deleted: 17

432 than  $10^5$  m,  $l_1$  is larger than  $l_2$  for the three different values of  $L$ , indicating an internal no-

433 flow boundary closer to the lagoon boundary. For example, taking  $L = 2000$  m and  $L_0 = 100$  m

434 leads to  $l_1 = 1240$  m and  $l_2 = 760$  m, with a deviation of 240 m (12% of 2000 m) from the

435 middle of the ASA. When  $L_0$  exceeds  $10^5$  m, however, the location of the internal no-flow

436 boundary can be approximated as being at the middle of the ASA for all considered values of

437  $L$ . This is in contrast to strip and circular aquifers where the internal no-flow boundary is

438 always in the middle of aquifer, due to symmetry.

Deleted: s

439 Since the internal no-flow boundary location between the sea and lagoon deviates from

440 the middle of the ASA, we expect aquifer geometry to play a significant role in controlling

447 seawater intrusion. As mentioned previously, ASAs can be convergent (Unit 1) or divergent  
448 aquifers (Unit 2) where the extent of seawater intrusion may be different. However, for strip  
449 aquifers, both Units 1 and 2 are rectangular with the same extent of seawater intrusion.  
450 Therefore, three geometries were compared in this study: convergent, rectangular and  
451 divergent (Figure 5). These geometries have been widely examined in hillslope hydrology  
452 regarding to the effects of aquifer geometry on runoff generation (Troch et al., 2003; Kong et  
453 al., 2016; Luo et al., 2018). To present the results more conveniently, we placed the  $r$ - $z$   
454 coordinate origin at the intersection of the constant-head boundary (sea or lagoon) and the  
455 impermeable base, with the  $r$ -axis pointing horizontally to the internal no-flow boundary and  
456 the  $z$ -axis vertically upward (Figure 5). In addition, the distance between the constant-head  
457 boundary and the internal no-flow boundary (aquifer width) is denoted as  $L^*$  (Figure 5) while  
458 the other parameters remain the same.

459 Following previous studies (e.g., Lu et al., 2016; 2019), different cases were selected to  
460 show the effects of aquifer geometry on seawater intrusion (Cases 1 and 2 in Table 1).  
461 According to Werner et al. (2017), the width of atoll islands generally varies from 100 to 1500  
462 m along the radial direction. In order to focus on the effects of aquifer geometry on seawater  
463 intrusion, the same  $L^*$  and  $L_0$  were assumed for the three aquifers, with  $L^*$  and  $L_0$  equal to  
464 1000 and 200 m, respectively. Note that  $L_0$  is the distance from the circle center to the lagoon  
465 boundary for convergent aquifers, whereas it represents the distance from the circle center to  
466 internal no-flow boundary for divergent aquifers hereafter. The sand characteristics were the  
467 same as in the experiments of Memari et al. (2020). Two recharge events were considered

Deleted: re

Deleted: x

Deleted: x



471 (Cases 1 and 2, Table 1). The freshwater-seawater interface was calculated using the  
472 analytical solutions for the three different aquifers. Note that the Appendix presents analytical  
473 solutions for seawater intrusion in strip aquifers deduced from Lu et al. (2019).

474 Figure 6 shows the freshwater-seawater interface calculated for Cases 1 and 2. As can be  
475 seen, the extent of seawater intrusion is noticeably different for the three aquifer geometries.  
476 For high recharge ( $1 \times 10^{-6} \text{ m s}^{-1}$ ), the interface tip is located at around 500 m for the  
477 divergent aquifer, which is about twice the value of the rectangular aquifer and six times the  
478 value for the convergent aquifer (Figure 6a). When the recharge decreases to  $3 \times 10^{-7} \text{ m s}^{-1}$ ,  
479 the interface tip moves further landward for the three aquifers as expected, but the difference  
480 between results is still great (Figure 6b). The interface tip is displaced above the aquifer bed  
481 for both the rectangular and divergent aquifers, while it remains on the aquifer bed for the  
482 convergent aquifer. Regardless of the recharge rate, the most landward freshwater-seawater  
483 interface occurs in the divergent aquifer and vice versa for the convergent aquifer. This  
484 underlines that aquifer geometry plays a major role in controlling seawater intrusion and  
485 hence it is necessary to account for aquifer geometry in analyses of seawater intrusion.

#### 486 **4.3. Sensitivity Analysis**

487 A sensitivity analysis was conducted to investigate to what extent aquifer geometry  
488 affects seawater intrusion. Since we focus on the effects of aquifer geometry on the locations  
489 of the freshwater-seawater interface and watertable, values of  $L_0$  and  $L^*$  were varied, with  
490 other parameters kept constant. When conducting the sensitivity analysis of  $L_0$ ,  $L^*$  was fixed  
491 at 1000 m, which is a typical value for ASAs (Werner et al., 2017). Figure 7 shows the

492 sensitivity of the locations of the freshwater-seawater interface and watertable to changes in  
493  $L_0$  (Case 3, Table 1). The freshwater-seawater interface and watertable elevation are  
494 independent of  $L_0$  for rectangular aquifers (Appendix). However, the freshwater-seawater  
495 interface and watertable elevation differ greatly when varying  $L_0$  for both convergent and  
496 divergent aquifers, highlighting that  $L_0$  plays an important role in affecting seawater intrusion.  
497 Specifically, as  $L_0$  increases, the freshwater-seawater interface moves more landward (larger  
498  $r/L^*$ , Figure 7a) and its corresponding watertable elevation decreases (Figure 7c) for  
499 convergent aquifers. In contrast, for divergent aquifers increasing  $L_0$  moves the freshwater-  
500 seawater interface more seaward (smaller  $r/L^*$ , Figure 7b) and its corresponding watertable  
501 elevation increases (Figure 7d). For a given  $L_0$ , divergent aquifers have the largest extent of  
502 seawater intrusion and the lowest watertable elevation, and conversely for convergent aquifers  
503 (Figure 7).

504 Regardless of the freshwater-seawater interface and watertable elevation, the deviation  
505 between rectangular aquifers and divergent or convergent aquifers is significant when  $L_0$  is  
506 less than 2000 m (Figure 7). For example, the  $r$ -coordinate of the interface tip ( $z = 0$ ) is 262 m  
507 for the rectangular aquifer at  $L_0 = 200$  m, whereas it is 78 (31% of that in the rectangular  
508 aquifer) and 500 m (191% of that in the rectangular aquifer) for the convergent and divergent  
509 aquifers, respectively. As  $L_0$  increases, the deviation between the three aquifers decreases.

510 When  $L_0 = 2000$  m, the  $r$ -coordinate of the interface tip is 262, 209 (80% of that in the  
511 rectangular aquifer) and 318 m (121% of that in the rectangular aquifer) for the rectangular,  
512 convergent and divergent aquifers, respectively. As  $L_0$  increases to 6000 m, the freshwater-

Deleted: x

Deleted: x

Deleted: x

Deleted: x

517 seawater interface and watertable elevation of both convergent and divergent aquifers tend to  
518 those of rectangular aquifers, i.e., geometry effects decrease with increasing  $L_0$ . These results  
519 highlight the critical role played by the shape of aquifers. As a result, ignoring the aquifer  
520 geometry may lead to an inappropriate management strategy for groundwater resources in  
521 atoll islands.

522 The sensitivity of the freshwater-seawater interface and watertable elevation to  $L^*$  was  
523 investigated by varying  $L^*$  from 600 to 1600 m while fixing  $L_0$  to 200 m (Case 4, Table 1). As  
524 shown in Figure 8, contrary to the results for varying  $L_0$ , in this case the freshwater-seawater  
525 interface and watertable elevation in all three topographies are related to  $L^*$ . Again, the extent  
526 of seawater intrusion is greatest in divergent aquifers and least in convergent aquifers for  
527 given  $L^*$ . When  $L^*$  increases, the freshwater-seawater interface moves seaward and the  
528 watertable elevation increases, regardless of aquifer geometry, i.e., the seawater intrusion  
529 decreases (Figures 8a-c). This is because the total freshwater flux increases with increasing  
530  $L^*$ , leading to a higher hydraulic gradient and hence less seawater intrusion (Figures 8d-f).  
531 Moreover, an increase in  $L^*$  reduces the differences in the seawater intrusion distance among  
532 the three geometries, i.e., the effects of aquifer geometry on seawater intrusion are more  
533 significant at small  $L^*$ . However, even at the maximum  $L^*$  considered (1600 m), the deviation  
534 between three aquifers remains significant: The  $x$ -coordinate of the interface tip is about 148  
535 m for the rectangular aquifer, whereas it is about 32 (22% of that in the rectangular aquifer)  
536 and 278 m (188% of that in the rectangular aquifer) for the convergent and divergent aquifers,  
537 respectively. Both  $L_0$  and  $L^*$  can greatly impact seawater intrusion estimates for divergent and

Deleted:  $x$

539 convergent aquifers, highlighting the necessity to include geometry effects in analytical  
540 solutions of seawater intrusion.

## 541 **5. Conclusions**

542 Based on the Ghijben-Herzberg and hillslope-storage Boussinesq equations, we derived  
543 analytical solutions of steady-state seawater intrusion for ASAs, with a focus on the  
544 freshwater-seawater interface and its corresponding watertable elevation as affected by  
545 recharge. After comparing with experimental data of Memari et al. (2020), the analytical  
546 solutions were employed to examine the effects of aquifer geometry on seawater intrusion in  
547 island aquifers. Three different shapes of island aquifer were compared: convergent,  
548 rectangular and divergent. The results lead to the following conclusions:

- 549 • The presented analytical solutions perform well in predicting the experimental freshwater-  
550 seawater interface, suggesting that these analytical solutions can predict seawater intrusion  
551 reasonably in different aquifer geometries.
- 552 • Island geometry plays a significant role in affecting the freshwater-seawater interface and  
553 watertable elevation. Other factors being equal, the extent of seawater intrusion is greatest  
554 in divergent aquifers, and conversely least in convergent aquifers. In contrast, the  
555 watertable elevation is lowest in divergent aquifers and highest in convergent aquifers.
- 556 • The effects of aquifer geometry on seawater intrusion are dependent on the aquifer width  
557 and distance from the circle center to the internal no-flow boundary (Figures 7 and 8). A  
558 larger aquifer width and distance from the circle center to the inner arc (the lagoon  
559 boundary for convergent aquifers ~~or the internal no-flow boundary for divergent aquifers~~)

Deleted: while

561 weaken, the role played by aquifer geometry and hence lead to a smaller deviation of the  
562 extent of seawater intrusion between the three topographies.

Deleted: s

563 Real island aquifers are expected to exhibit more complexity than considered here, e.g.,

564 they will have more complex shapes and are subjected to transient flow conditions caused by  
565 tides, waves and groundwater pumping (Mantoglou et al. 2003; Pool & Carrera., 2011;

Deleted: at

566 Werner et al., 2013). In addition, since the experimental scale of Memari et al. (2020) is

567 necessarily small, future experiments and field data are needed to further validate and

568 facilitate the analytical solutions. Despite this, the new analytical solutions, validated against

569 experiments, can be used as a tool for rapid estimation of seawater intrusion in ASAs once

570 known island geometry and corresponding soil properties are given.

573 **Appendix: Analytical Solutions for Rectangular Aquifers**

574 For rectangular aquifers, the seawater intrusion in Unit 1 is identical to that in Unit 2  
575 because of symmetry. With the interface tip on the aquifer bed, analytical solutions for the  
576 freshwater-seawater interface ( $h_s$ ), watertable elevation ( $h$ ), and  $r$ -coordinate of the interface  
577 tip in Unit 2 ( $r_{i2}$ ) can be respectively written as (Lu et al., 2019),

$$578 \quad h_s = \alpha \sqrt{\frac{N}{(1+\alpha)K_s} \left( \frac{L^2}{4} - r^2 \right)} \quad (A1)$$

$$579 \quad h = \begin{cases} \sqrt{\frac{N}{K_s} (r_{i2}^2 - r^2) + \left( \frac{H_s}{\alpha} + H_s \right)} & 0 \leq r \leq r_{i2} \\ \sqrt{\frac{N}{(1+\alpha)K_s} \left( \frac{L^2}{4} - r^2 \right) + H_s} & r_{i2} < r \leq \frac{L}{2} \end{cases} \quad (A2)$$

$$580 \quad r_{i2} = \sqrt{\frac{L^2}{4} - \frac{(1+\alpha)K_s}{N} \left( \frac{H_s^2}{\alpha^2} \right)} \quad (A3)$$

581 When the interface tip is above the aquifer bed, the analytical solution for the freshwater-  
582 seawater interface location and watertable elevation in Unit 2 are the same as equations (A1)  
583 and (A2), respectively.

Deleted: x

Deleted:  $x_{i2}$

586

**Code/Data availability**

587

Experimental data used in this study ~~were~~ compiled from Memari et al. (2020).

Deleted: a

589 **Author contributions**

590 All authors contributed to the design of the research. ZL carried out data collation,  
591 developed the analytical solutions and prepared the manuscript with contributions from all  
592 co-authors. All authors contributed to the interpretation of the results and provided feedback.



593 **Competing interests**

594 The authors declare that they have no conflicts of interest.

595 **Acknowledgments**

596 This research was supported by the National Key R&D Program of China  
597 (2019YFC0409004) and the National Natural Science Foundation of China (51979095 and  
598 41807178). ZL acknowledges EPFL for financial support and JK acknowledges the Qing Lan  
599 Project of Jiangsu Province (2020). We appreciate the constructive comments from the  
600 handling Editor Mauro Giudici and three anonymous reviewers, which led to significant  
601 improvement of the paper.

Deleted: review

## References

- Ayers, J. F., & Vacher, H. L. (1986). Hydrogeology of an atoll island: A conceptual model from detailed study of a Micronesian example. *Groundwater*, 24(2), 185-198.  
<https://doi.org/10.1111/j.1745-6584.1986.tb00994.x>
- Bailey, R. T., Jenson, J. W., & Olsen, A. E. (2010). Estimating the ground water resources of atoll islands. *Water*, 2(1), 1-27. <https://doi.org/10.3390/w2010001>
- Bailey, R. T., Jenson, J. W., & Olsen, A. E. (2009). Numerical modeling of atoll island hydrogeology. *Groundwater*, 47(2), 184-196. <https://doi.org/10.1111/j.1745-6584.2008.00520.x>
- Bedekar, V. S., Memari, S. S., & Clement, T. P. (2019). Investigation of transient freshwater storage in island aquifers. *Journal of Contaminant Hydrology*, 221, 98-107.  
<https://doi.org/10.1016/j.jconhyd.2019.02.004>
- Chesnaux, R., & Allen, D. M. (2008). Groundwater travel times for unconfined island aquifers bounded by freshwater or seawater. *Hydrogeology Journal*, 16(3), 437-445.  
<https://doi.org/10.1007/s10040-007-0241-6>
- Dose, E. J., Stoeckl, L., Houben, G. J., Vacher, H. L., Vassolo, S., Dietrich, J., & Himmelsbach, T. (2014). Experiments and modeling of freshwater lenses in layered aquifers: Steady state interface geometry. *Journal of Hydrology*, 509, 621-630.  
<https://doi.org/10.1016/j.jhydrol.2013.10.010>
- Drabbe J. & Badon Ghijben, W. (1889). *Nota in verband met de voorgenomen put boring nabij Amsterdam*. Tijdschrift van het Koninklijk Instituut van Ingenieurs. pp. 8-22,

624 Gravenhage, Netherlands.

625 Duvat, V. K. E. (2019). A global assessment of atoll island planform changes over the past  
626 decades. *Wiley Interdisciplinary Reviews: Climate Change*, 10(1), e557.

627 <https://doi.org/10.1002/wcc.557>

628 Fan, Y., & Bras, R. L. (1998). Analytical solutions to hillslope subsurface storm flow and  
629 saturation overland flow. *Water Resources Research*, 34(4), 921-927.

630 <https://doi.org/10.1029/97WR03516>

631 Fetter, C. W. (1972). Position of the saline water interface beneath oceanic islands. *Water*  
632 *Resources Research*, 8(5), 1307-1315. <https://doi.org/10.1029/WR008i005p01307>

633 Gingerich, S. B., Voss, C. I., & Johnson, A. G. (2017). Seawater-flooding events and impact  
634 on freshwater lenses of low-lying islands: Controlling factors, basic management and  
635 mitigation. *Journal of Hydrology*, 551, 676-688.

636 <https://doi.org/10.1016/j.jhydrol.2017.03.001>

637 Greskowiak, J., Röper, T., & Post, V. E. (2013). Closed-form approximations for two-  
638 dimensional groundwater age patterns in a fresh water lens. *Groundwater*, 51(4), 629-  
639 634. <https://doi.org/10.1111/j.1745-6584.2012.00996.x>

640 Hazenberg, P., Fang, Y., Broxton, P., Gochis, D., Niu, G. Y., Pelletier, J. D., Troch., P. A., &  
641 Zeng, X. (2015). A hybrid-3D hillslope hydrological model for use in Earth system  
642 models. *Water Resources Research*, 51(10), 8218-8239.

643 <https://doi.org/10.1002/2014WR016842>

644 Hazenberg, P., Broxton, P., Gochis, D., Niu, G. Y., Pangle, L. A., Pelletier, J. D., Troch., P. A.,

Formatted: Font: 小四

Formatted: Normal, Indent: Hanging: 2.95 ch,  
Left 0.01 ch, First line: -2.95 ch

Formatted: Font: 小四, Italic

Formatted: Font: 小四

Formatted: Font: 小四, Italic

Formatted: Font: 小四

645 & Zeng, X. (2016). Testing the hybrid-3-D hillslope hydrological model in a  
646 controlled environment. *Water Resources Research*, 52(2), 1089-1107.  
647 <https://doi.org/10.1002/2015WR018106>

648 Herzberg, A. (1901). Die wasserversorgung einiger Nordseebäder. *Journal für*  
649 *Gasbeleuchtung und Wasserversorgung*, 44, 815-819, 45, 842-844.

650 Hilberts, A. G. J., Troch, P. A., & Paniconi, C. (2005). Storage-dependent drainable porosity  
651 for complex hillslopes. *Water Resources Research*, 41(6), W06001.  
652 <https://doi.org/10.1029/2004WR003725>

653 Hilberts, A. G., Troch, P. A., Paniconi, C., & Boll, J. (2007). Low-dimensional modeling of  
654 hillslope subsurface flow: Relationship between rainfall, recharge, and unsaturated  
655 storage dynamics. *Water Resources Research*, 43(3), W03445.  
656 <https://doi.org/10.1029/2006WR004964>

657 Ketabchi, H., Mahmoodzadeh, D., Ataie-Ashtiani, B., Werner, A. D., & Simmons, C. T.  
658 (2014). Sea-level rise impact on fresh groundwater lenses in two-layer small islands.  
659 *Hydrological Processes*, 28(24), 5938-5953. <https://doi.org/10.1002/hyp.10059>

660 Kong, J., Shen, C., Luo, Z., Hua, G., & Zhao, H. (2016). Improvement of the hillslope-storage  
661 Boussinesq model by considering lateral flow in the unsaturated zone. *Water*  
662 *Resources Research*, 52(4), 2965-2984. <https://doi.org/10.1002/2015WR018054>

663 Lam, R. K. (1974). Atoll permeability calculated from tidal diffusion. *Journal of Geophysical*  
664 *Research*, 79(21), 3073-3081. <https://doi.org/10.1029/JC079i021p03073>

665 Liu, J., & Tokunaga, T. (2019). Future risks of tsunami-induced seawater intrusion into

666 unconfined coastal aquifers: Insights from numerical simulations at Niijima Island,  
667 Japan. *Water Resources Research*, 55(12), 10082-10104.  
668 <https://doi.org/10.1029/2019WR025386>

669 Liu, Y., X. Mao, J. Chen, and D. A. Barry. 2014. Influence of a coarse interlayer on seawater  
670 intrusion and contaminant migration in coastal aquifers. *Hydrological Processes*, 28(20),  
671 5162-5175. <https://dx.doi.org/10.1002/hyp.10002>

672 Lu, C., Cao, H., Ma, J., Shi, W., Rathore, S. S., Wu, J., & Luo, J. (2019). A proof-of-concept  
673 study of using a less permeable slice along the shoreline to increase fresh groundwater  
674 storage of oceanic islands: Analytical and experimental validation. *Water Resources  
675 Research*, 55(8), 6450-6463. <https://doi.org/10.1029/2018WR024529>

676 Lu, C., Xin, P., Kong, J., Li, L., & Luo, J. (2016). Analytical solutions of seawater intrusion in  
677 sloping confined and unconfined coastal aquifers. *Water Resources Research*, 52(9),  
678 6989-7004. <https://doi.org/10.1002/2016WR019101>

679 Luo, Z., Shen, C., Kong, J., Hua, G., Gao, X., Zhao, Z., Zhao, H., & Li, L. (2018). Effects of  
680 unsaturated flow on hillslope recession characteristics. *Water Resources Research*,  
681 54(3), 2037-2056. <https://doi.org/10.1002/2017WR022257>

682 Mantoglou, A. (2003). Pumping management of coastal aquifers using analytical models of  
683 saltwater intrusion. *Water Resources Research*, 39(12), 1335.  
684 <https://doi.org/10.1029/2002WR001891>

685 Memari, S. S., Bedekar, V. S., & Clement, T. P. (2020). Laboratory and numerical  
686 investigation of saltwater intrusion processes in a circular island aquifer. *Water*

687 *Resources Research*, 56(2), e2019WR025325. <https://doi.org/10.1029/2019WR025325>

688 Morgan, L. K., & Werner, A. D. (2014). Seawater intrusion vulnerability indicators for  
689 freshwater lenses in strip islands. *Journal of Hydrology*, 508, 322-327.  
690 <https://doi.org/10.1016/j.jhydrol.2013.11.002>

691 Paniconi, C., Troch, P. A., Van Loon, E. E., & Hilberts, A. G. (2003). Hillslope-storage  
692 Boussinesq model for subsurface flow and variable source areas along complex  
693 hillslopes: 2. Intercomparison with a three-dimensional Richards equation model.  
694 *Water Resources Research*, 39(11), 1317. <https://doi.org/10.1029/2002WR001730>

695 Pool, M., & Carrera, J. (2011). A correction factor to account for mixing in Ghyben-Herzberg  
696 and critical pumping rate approximations of seawater intrusion in coastal aquifers.  
697 *Water Resources Research*, 47(5), W05506. <https://doi.org/10.1029/2010WR010256>

698 Post, V. E. (2018). Annotated translation of “Nota in verband met de voorgenomen putboring  
699 nabij Amsterdam [Note concerning the intended well drilling near Amsterdam]” by J.  
700 Drabbe and W. Badon Ghijben (1889). *Hydrogeology Journal*, 26(6), 1771-1788.  
701 <https://doi.org/10.1007/s10040-018-1797-z>

702 Post, V. E. A., Houben, G. J., Stoeckl, L., & Sültenfuß, J. (2019). Behaviour of tritium and  
703 tritiogenic helium in freshwater lens groundwater systems: Insights from Langeoog  
704 Island, Germany. *Geofluids*, Volume 2019, Article ID 1494326.  
705 <https://doi.org/10.1155/2019/1494326>

706 Röper, T., Greskowiak, J., Freund, H., & Massmann, G. (2013). Freshwater lens formation  
707 below juvenile dunes on a barrier island (Spiekeroog, Northwest Germany). *Estuarine*,

708 *Coastal and Shelf Science*, 121-122, 40-50. <https://doi.org/10.1016/j.ecss.2013.02.004>

709 Stoeckl, L., Houben, G. J., & Dose, E. J. (2015). Experiments and modeling of flow processes  
710 in freshwater lenses in layered island aquifers: Analysis of age stratification, travel  
711 times and interface propagation. *Journal of Hydrology*, 529, 159-168.  
712 <https://doi.org/10.1016/j.jhydrol.2015.07.019>

713 Storlazzi, C. D., Gingerich, S. B., van Dongeren, A., Cheriton, O. M., Swarzenski, P. W.,  
714 Quataert, E., Voss, C. I., Field, D. W., Annamalai, H., Piniak, G. A., & McCall, R.  
715 (2018). Most atolls will be uninhabitable by the mid-21st century because of sea-level  
716 rise exacerbating wave-driven flooding. *Science Advances*, 4(4), eaap9741.  
717 <https://doi.org/10.1126/sciadv.aap9741>

718 Strack, O. D. L. (1976). A single-potential solution for regional interface problems in coastal  
719 aquifers. *Water Resources Research*, 12(6), 1165-1174.  
720 <https://doi.org/10.1029/WR012i006p01165>

721 Stuyfzand, P. J. (2017). Observations and analytical modeling of freshwater and rainwater  
722 lenses in coastal dune systems. *Journal of Coastal Conservation*, 21(5), 577-593.  
723 <https://doi.org/10.1007/s11852-016-0456-6>

724 Stuyfzand, P. J. (1993). *Hydrochemistry and hydrology of the coastal dune area of the Western*  
725 *Netherlands*. Ph.D. Thesis. Vrije University, Amsterdam, KIWA, ISBN 90-74741-01-  
726 0. <http://dare.ubvu.vu.nl/handle/1871/12716>

727 Thomas, A., Baptiste, A., Martyr-Koller, R., Pringle, P., & Rhiney, K. (2020). Climate change  
728 and small island developing states. *Annual Review of Environment and Resources*,



729 45(1), 1-27. <https://doi.org/10.1146/annurev-environ-012320-083355>

730 Troch, P. A., Paniconi, C., & Emiel van Loon, E. (2003). Hillslope-storage Boussinesq model  
731 for subsurface flow and variable source areas along complex hillslopes: 1.  
732 Formulation and characteristic response. *Water Resources Research*, 39(11), 1316.  
733 <https://doi.org/10.1029/2002WR001728>

734 Underwood, M. R., Peterson, F. L., & Voss, C. I. (1992). Groundwater lens dynamics of atoll  
735 islands. *Water Resources Research*, 28(11), 2889-2902.  
736 <https://doi.org/10.1029/92WR01723>

737 Vacher, H. L. 1988. Dupuit-Ghyben-Herzberg analysis of strip-island lenses. *Geological*  
738 *Society of America Bulletin*, 100, 580-591. [https://doi.org/10.1130/0016-](https://doi.org/10.1130/0016-7606(1988)100<0580:DGHAOS>2.3.CO;2)  
739 [7606\(1988\)100<0580:DGHAOS>2.3.CO;2](https://doi.org/10.1130/0016-7606(1988)100<0580:DGHAOS>2.3.CO;2)

740 Werner, A. D., Sharp, H. K., Galvis, S. C., Post, V. E., & Sinclair, P. (2017). Hydrogeology  
741 and management of freshwater lenses on atoll islands: Review of current knowledge  
742 and research needs. *Journal of Hydrology*, 551, 819-844.  
743 <https://doi.org/10.1016/j.jhydrol.2017.02.047>

744 Werner, A. D., Bakker, M., Post, V. E., Vandenbohede, A., Lu, C., Ataie-Ashtiani, B.,  
745 Simmons, C. T., & Barry, D. A. (2013). Seawater intrusion processes, investigation  
746 and management: Recent advances and future challenges. *Advances in Water*  
747 *Resources*, 51, 3-26. <https://doi.org/10.1016/j.advwatres.2012.03.004>

748 Werner, A. D., & Simmons, C. T. (2009). Impact of sea-level rise on sea water intrusion in  
749 coastal aquifers. *Groundwater*, 47(2), 197-204. <https://doi.org/10.1111/j.1745->

750 [6584.2008.00535.x](#)

751 White, I., & Falkland, T. (2010). Management of freshwater lenses on small Pacific islands.

752 *Hydrogeology Journal*, 18(1), 227-246. <https://doi.org/10.1007/s10040-009-0525-0>

753 Zhang, Y., Li, L., Erler, D. V., Santos, I., & Lockington, D. (2016). Effects of alongshore

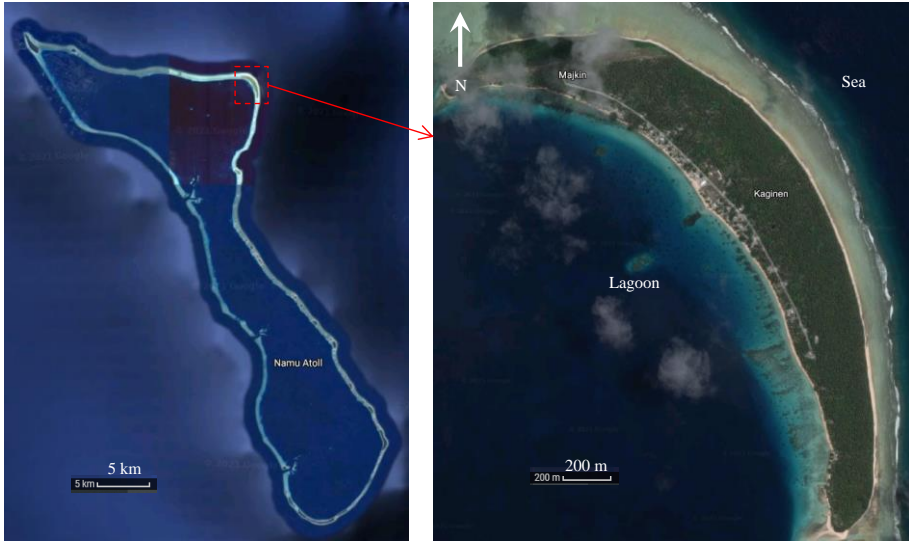
754 morphology on groundwater flow and solute transport in a nearshore aquifer. *Water*

755 *Resources Research*, 52(2), 990-1008. <https://doi.org/10.1002/2015WR017420>

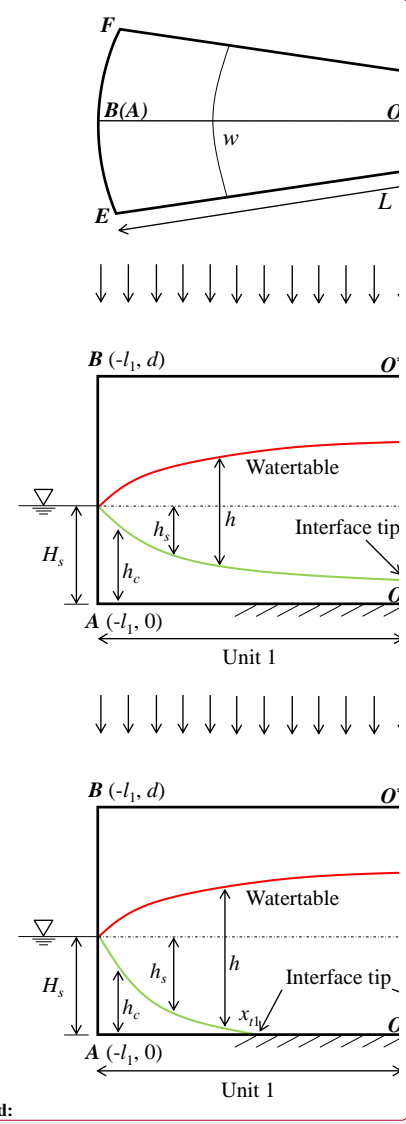
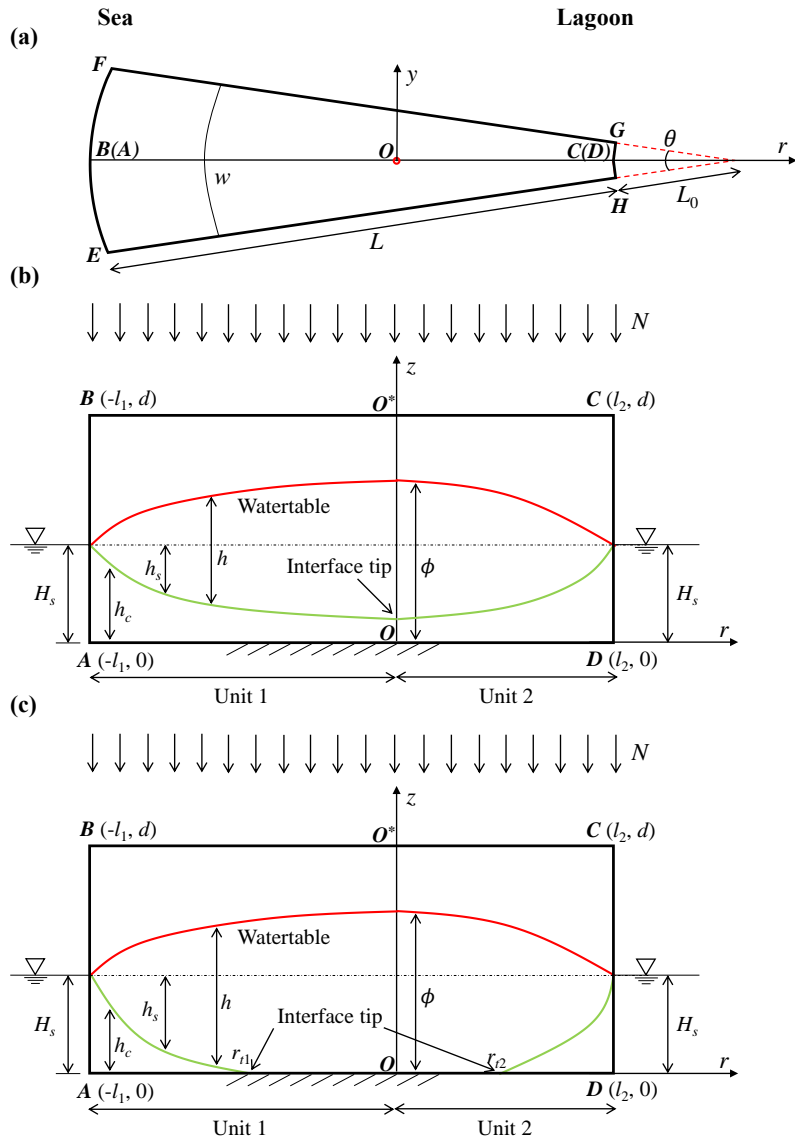
756 **Table 1.** List of parameters use in different simulations.

	No.	$L^*$ (m)	$L_0$ (m)	$H_s$ (m)	$d$ (m)	$\alpha$ (-)	$K_s$ (m s <sup>-1</sup> )	$N$ (m s <sup>-1</sup> )
Cases	1	1000	200	38	45	40	$1.23 \times 10^{-2}$	$1 \times 10^{-6}$
	2	1000	200	38	45	40	$1.23 \times 10^{-2}$	$3 \times 10^{-7}$
	3	1000	†	38	45	40	$1.23 \times 10^{-2}$	$1 \times 10^{-6}$
	4	†	200	38	45	40	$1.23 \times 10^{-2}$	$1 \times 10^{-6}$

757 †The parameter is varied: The range of  $L_0$  is from 200 to 6000 m, whereas the range of  $L^*$  is  
758 from 600 to 1600 m.



759  
760 **Figure 1.** Island with an annulus segment in the Namu Atoll, Marshall Islands (© Google  
761 Earth).



Deleted:

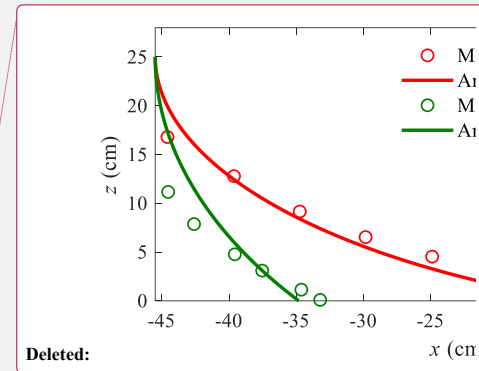
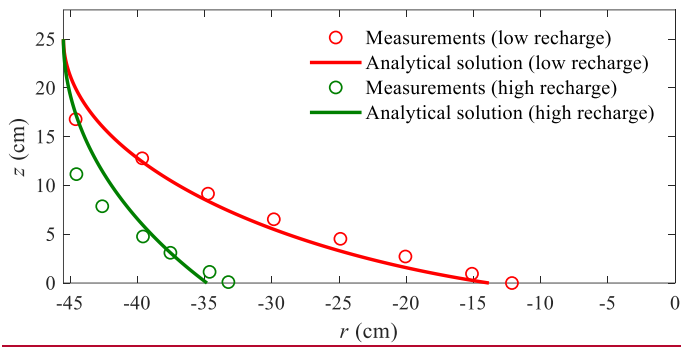
Formatted: Font: Not Bold

Deleted: side view

Formatted: Font color: Text 1

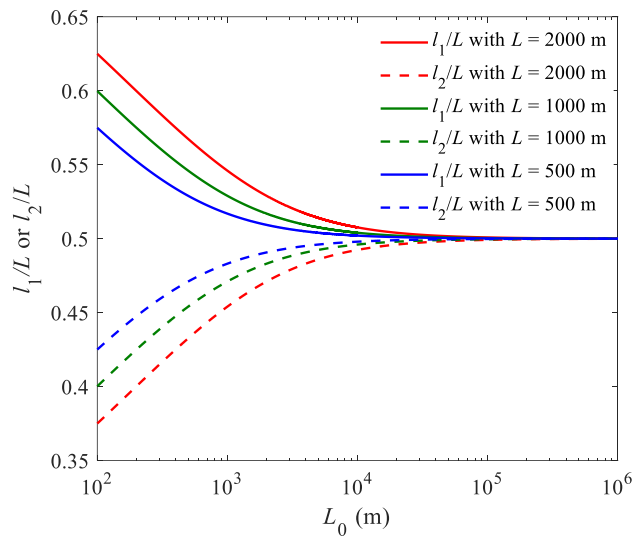
762  
763 **Figure 2.** Conceptual model of an annulus segment aquifer (a slice of an atoll island). (a) Plan  
764 view and (b, c) lateral vertical cross section with the saltwater interface tip (b) above the  
765 aquifer bed (single location) and (c) on the aquifer bed (two locations). In (a), the sea  
766 boundary is on  $EF$  and the atoll lagoon boundary is on  $HG$ ; In (b) and (c),  $AD$  is the

769 impermeable base and  $OO^*$  is the internal no-flow boundary.



770

771 **Figure 3.** Comparison between analytical and experimental (data compiled from Memari et  
 772 al., 2020) results for the freshwater-seawater interface location for different recharge events.  
 773 Note that the left and right sides are the sea and internal no-flow boundaries, respectively.



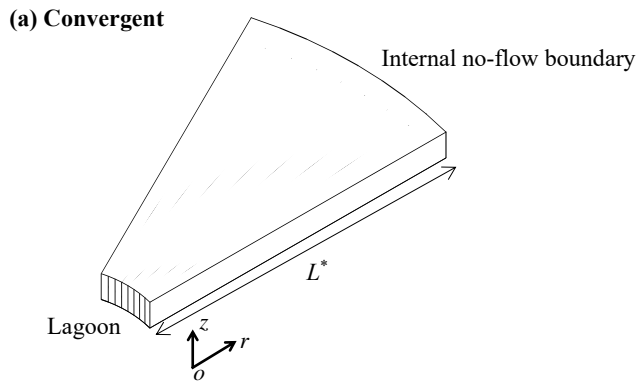
775

776

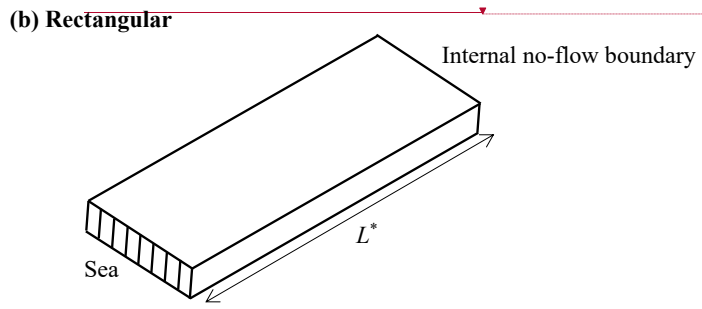
**Figure 4.** Widths of Unit 1 and Unit 2 versus  $L_0$  for aquifers with different total width  $L$ .



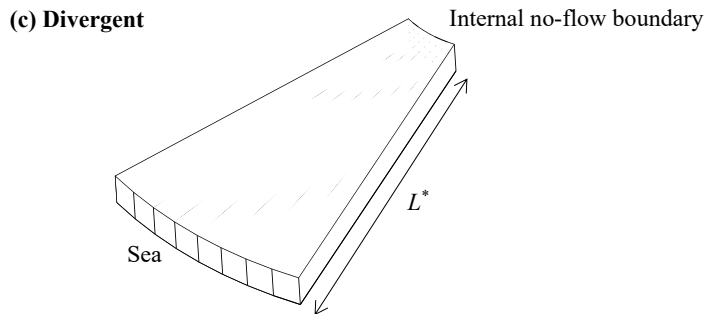
777



778



779



780

**Figure 5.** Three-dimensional view of (a) convergent (smaller side facing the lagoon), (b)

781

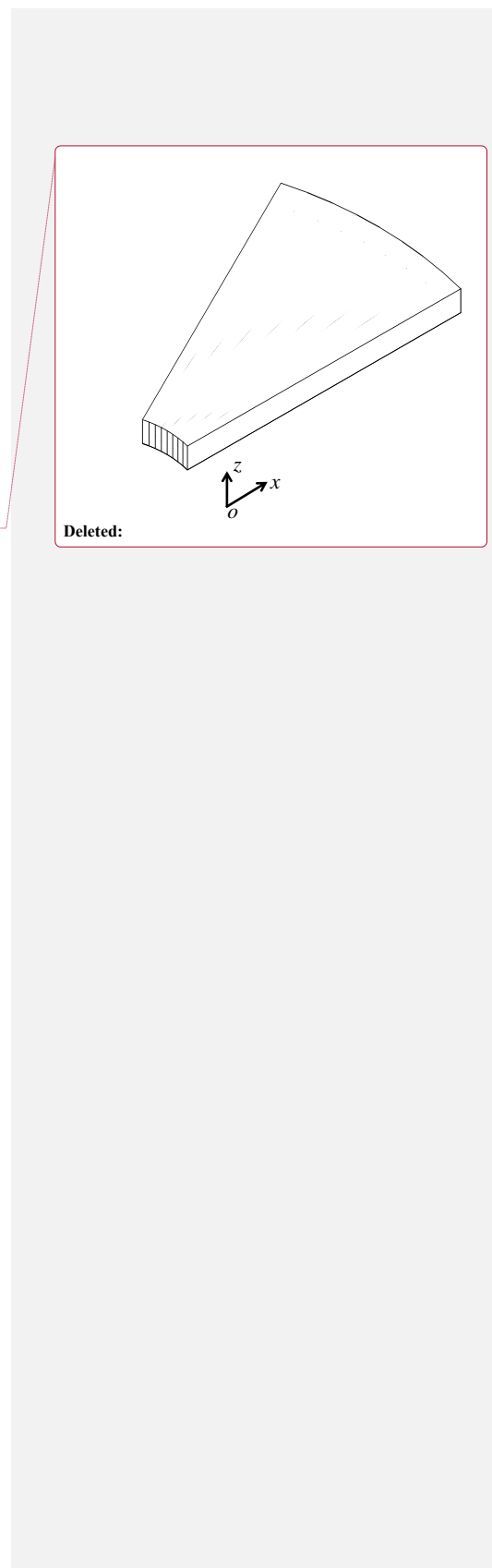
rectangular and (c) divergent aquifers (larger side facing the sea) compared in this study.  $L^*$

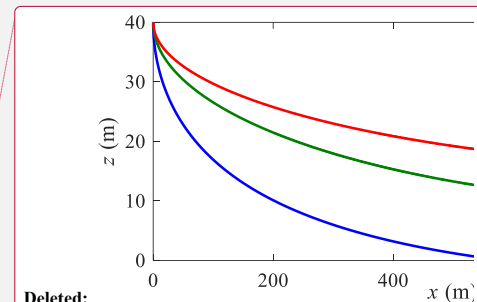
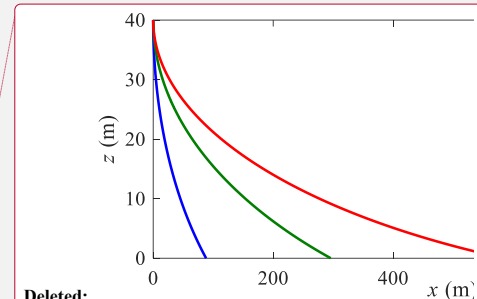
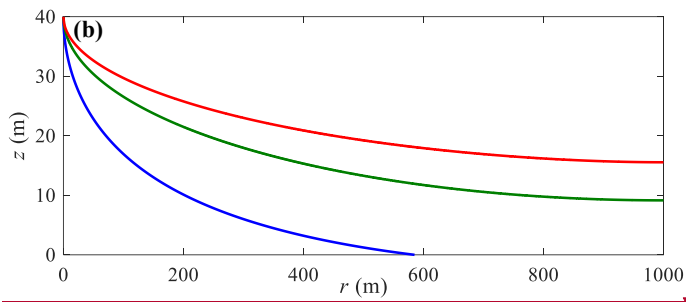
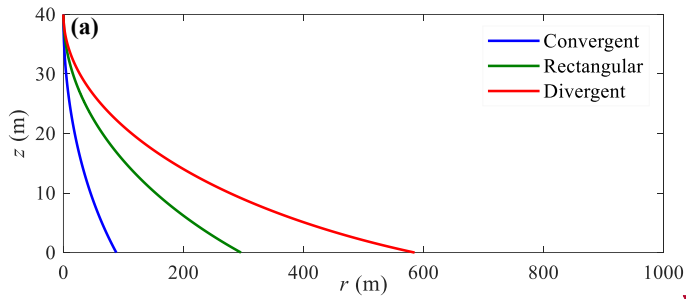
782

represents the distance from the sea/lagoon to the internal no-flow boundary, i.e.,  $l_1$  or  $l_2$  in

783

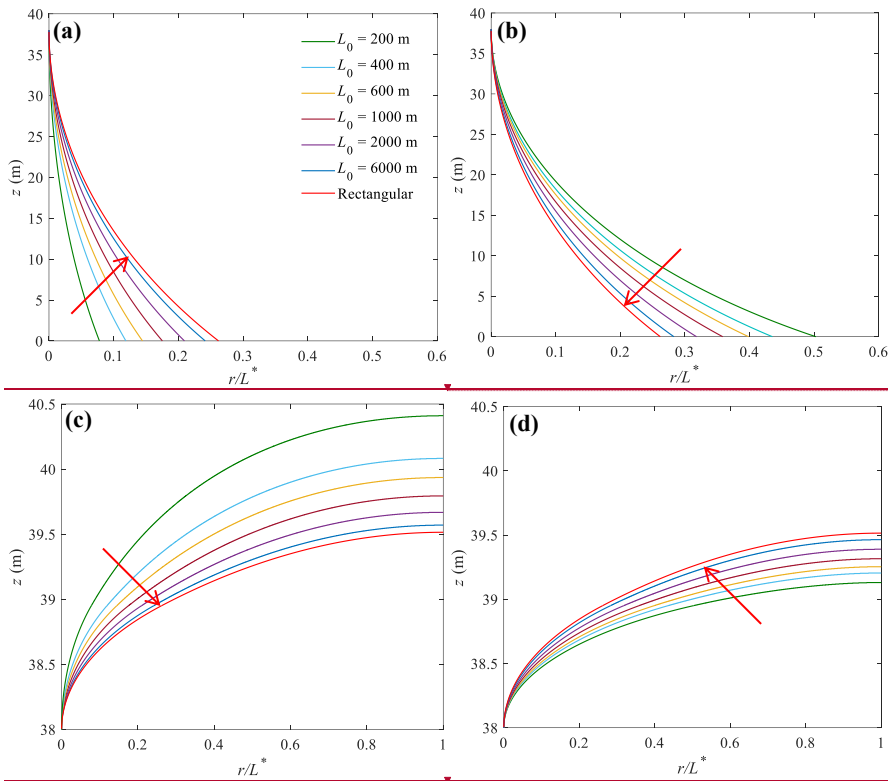
Figure 2. The internal no-flow boundary corresponds to the  $z$ -axis in Figure 2.



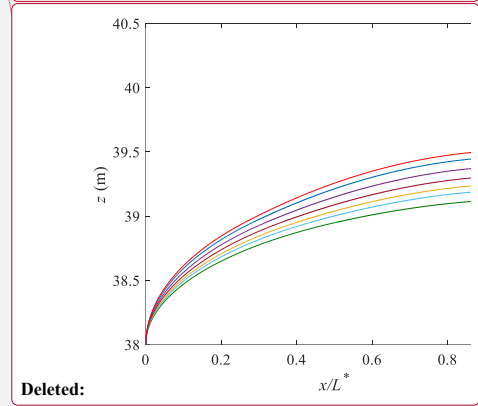
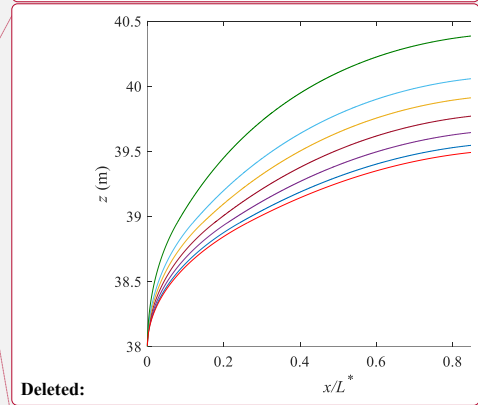
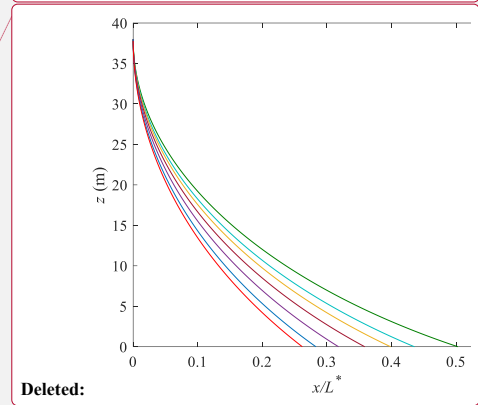
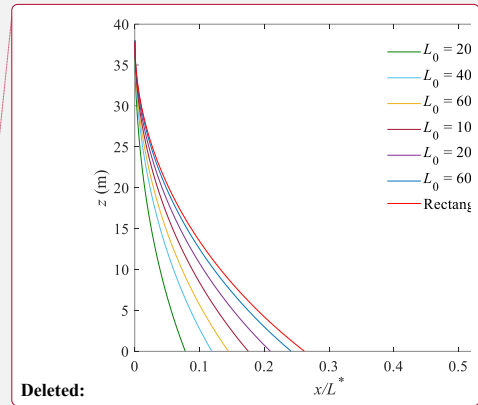


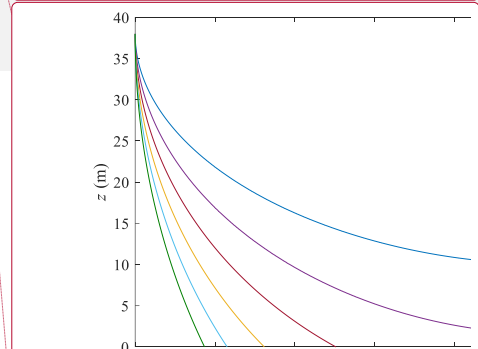
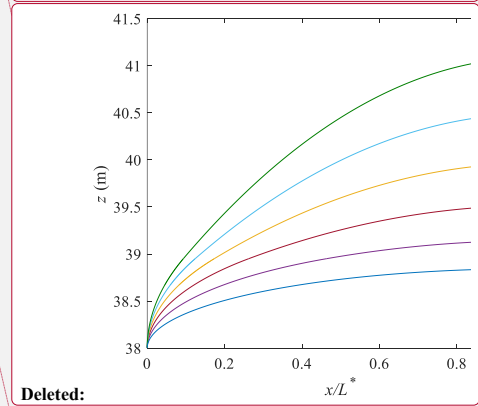
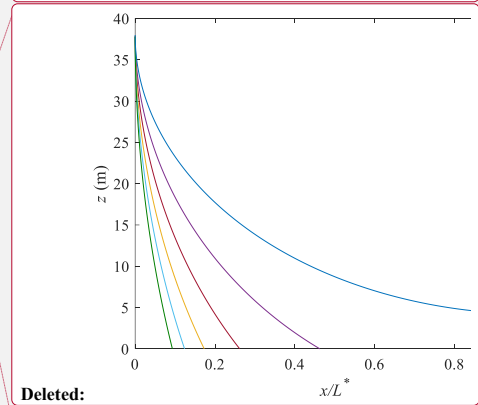
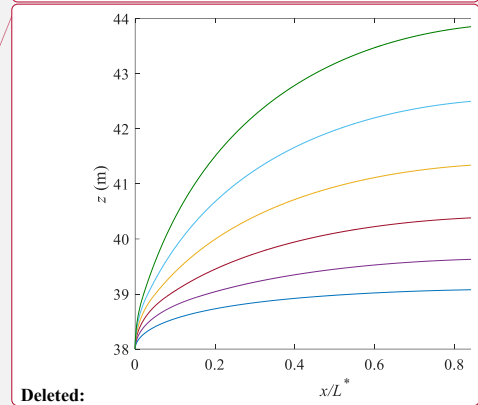
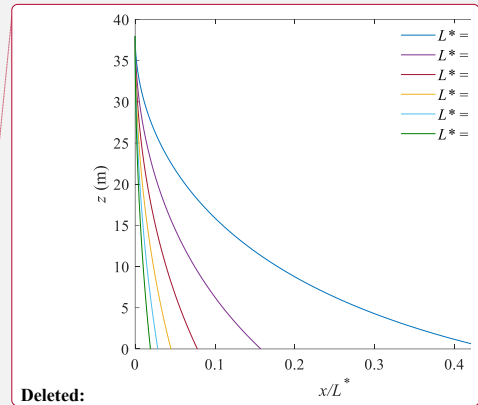
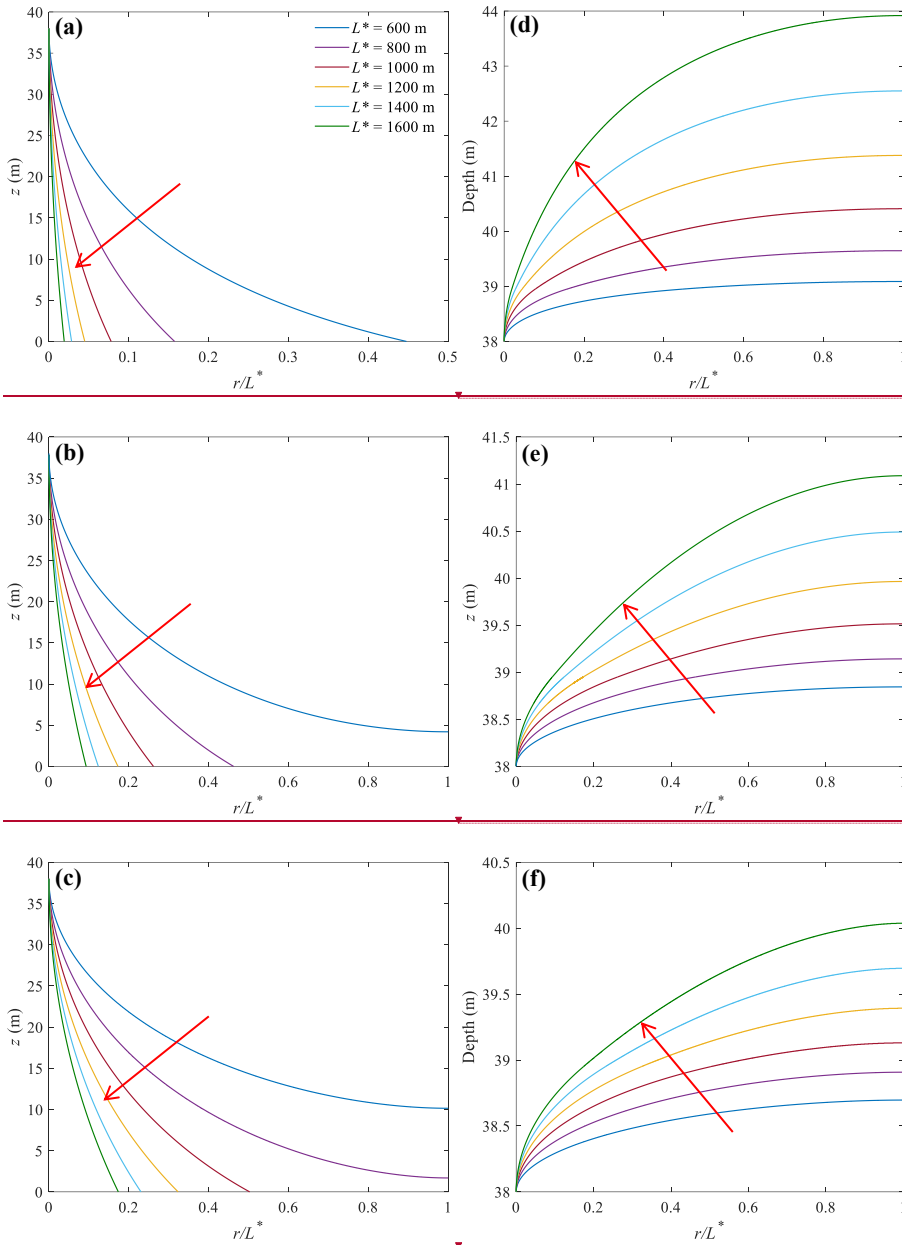
785  
786  
787 **Figure 6.** Freshwater-seawater interface predicted by analytical solutions for three different  
788 aquifers with (a) high and (b) low recharge (Cases 1 and 2 in Table 1). Note that  $r = 1000$  m is  
789 the internal no-flow boundary in Figure 5.

Deleted: x



795 **Figure 7.** Sensitivity of (a, b) the locations of the freshwater-seawater interface and (c, d)  
 796 watertable to  $L_0$  for convergent (left panel) and divergent (right panel) aquifers. The arrow in  
 797 each plot shows the direction of increasing  $L_0$  (values given in (a), used to produce the  
 798 different curves). Note that predictions for rectangular aquifers are independent of  $L_0$ .





807

808

809

810 **Figure 8.** Sensitivity of (a-c) the locations of the freshwater-seawater interface and (d-f)  
 811 watertable to  $L^*$  for convergent (a, d), rectangular (b, e) and divergent (c, f) aquifers. The

824 arrow in each plot points to the increase of  $L^*$  values used to construct each curve (values  
825 indicated in (a)).